Supplementary Information

Kinetically Programmed Pathway-Dependent Autonomous Reversibility in Biomimetic Self-Assembly of Nanoparticles

Sumit Roy, Shreya Tyagi, and Pramod P. Pillai*

Department of Chemistry,
Indian Institute of Science Education and Research (IISER),
Dr. Homi Bhabha Road, Pune 411 008, India

*Correspondence to: pramod.pillai@iiserpune.ac.in

Table of Contents:

Section 1:

Experimental details

Materials and Reagents

Tetrachloroaurate trihydrate ($HAuCl_4.3H_2O$), Hydrazine monohydrate ($N_2H_4.H_2O$ 50-60%), Hexokinase (HK), D-(+)-Glucose, dodecylamine (DDA) and tetrabutylammonium borohydride (TBAB) were purchased from Sigma-Aldrich. Adenosine-5′-triphosphate disodium salt hydrate (ATP), Adenosine-5′-diphosphate disodium salt hydrate (ADP), and (Di-n-dodecyl)-dimethyl-ammonium bromide (DDAB) were purchased from Alfa Aesar. All the reagents were used as received without any further purification. The positively charged N,N,N-trimethyl(11-mercaptoundecyl) ammonium ion (TMA) was synthesized, followed by a reported procedure.[1]

Synthesis of [+] AuNPs

[+] AuNPs were synthesized following a place exchange method.[2,3] First, dodecylamine (DDA) capped AuNPs were synthesized by a modified previous report.[2,3] $HAuCl_4.3H_2O$ and hydrazine monohydrate ($N_2H_4.H_2O$) were used as the gold precursor and the reducing agent, respectively. In the experiment, $HAuCl_4.3H_2O$ (11 mg), DDA (104 mg), and DDAB (129 mg) were mixed together in toluene (3.1 mL) and sonicated for ~10 min to stabilize the Au (III) ions. After that, another toluene solution (1.3 mL) containing 27.3 mg of TBAB and 51.7 mg of DDAB was rapidly injected for the complete reduction of Au (III) salt. The resulting seed solution was then aged overnight, and the seed particles were grown to 5.4 ± 0.5 nm. For that, a growth solution was prepared by mixing 550 mg of DDAB, 1.38 g of DDA, 117 mg of $HAuCl_4.3H_2O$, and 4.5 mL of seed solution in 30 mL toluene. After that, another toluene solution (12 mL) having 116 μL of $N_2H_4.H_2O$ and 750 mg of DDAB was added dropwise to reduce the growth solution. The final solution was kept overnight under stirring conditions for the complete growth of the particles. Finally, it yielded a monodisperse 5.4 ± 0.5 nm of DDA-AuNPs.

In a typical synthesis of [+] AuNP, 15 mL of DDA-AuNP was first purified through precipitation in 50 mL methanol, yielding a black precipitate. The supernatant was carefully removed, and the precipitate was then re-dispersed in 20 mL toluene. A ~40-fold molar excess of ligand (N,N,N-trimethyl(11-mercaptoundecyl)ammonium chloride (TMA, [+]), dissolved in 10 mL dichloromethane (DCM), was added during the place exchange. The solution was left

overnight for complete ligand exchange. After that, the supernatant was decanted, and the precipitate was washed with DCM (3×50 mL) and acetone (50 mL) to remove all the excess ligands. The precipitate was then dried and redispersed in milli-Q water. The synthesized [+] AuNPs showed a surface plasmon band of ~520 nm.

Preparation of [+] AuNPs

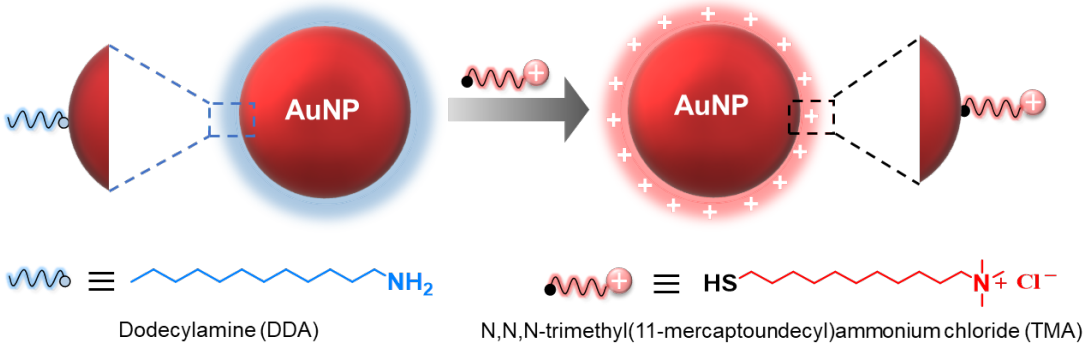

Figure S1. Schematics for the place exchange protocol. DDA-capped AuNPs were place exchanged with [+] TMA ligands to synthesize the positively charged AuNPs.

Characterization of [+] AuNPs

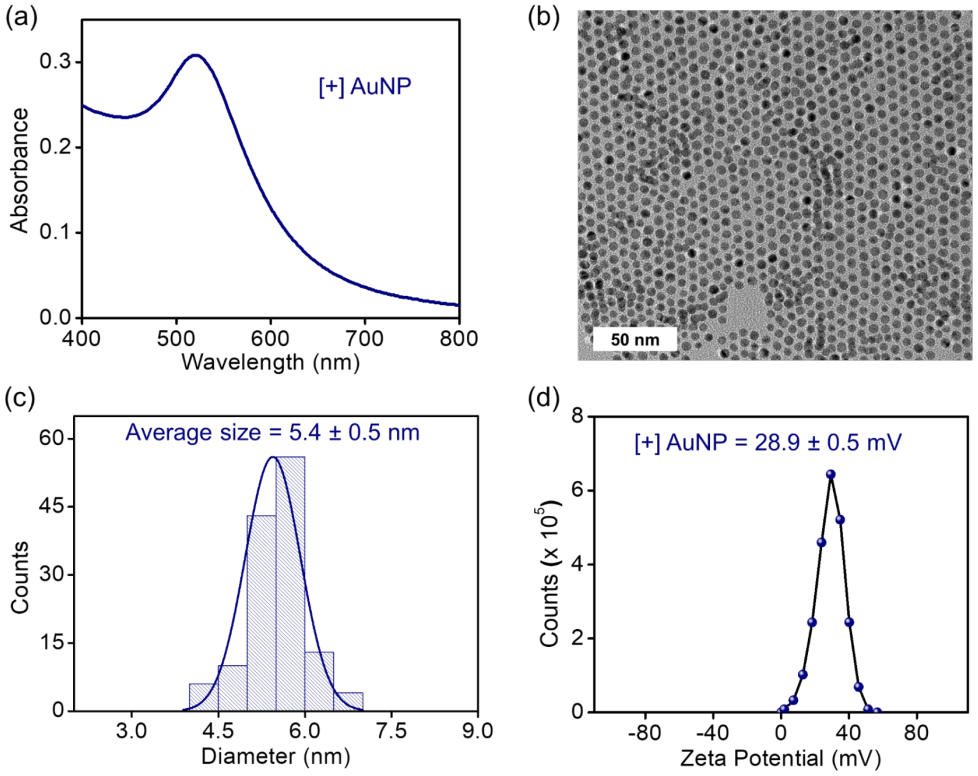

Figure S2. Absorption, TEM, and surface characterization of [+] AuNPs. **(a)** UV-vis absorption spectrum of [+] AuNPs. **(b)** A representative TEM image of [+] AuNPs, and **(c)** the corresponding size distribution histogram showing the average size to be 5.4±0.5 nm. **(d)** Typical zeta potential plot for [+] AuNPs. The error was estimated from three independent measurements.

Microscopy studies

Detailed microscopy (TEM and SEM) studies were performed in order to characterize the AuNP and to monitor the dynamic self-assembly process.

Transmission electron microscopy (TEM) study

TEM studies were performed to characterize the AuNPs and to monitor the enzyme-coupled dynamic self-assembly process. The TEM samples were prepared by drop casting the solution on a 400-mesh carbon-coated copper grid (Tedpella Inc.) and dried under vacuum before imaging. Finally, the TEM images were recorded on a JEOL JEM-2200FS HRTEM instrument.

Scanning electron microscopy (SEM) study

SEM studies were performed to characterize the AuNPs and also to monitor the dynamic self-assembly process. The SEM samples were prepared by drop casting the solution on a Si wafer substrate and kept for drying under a vacuum. Finally, FE-SEM images were recorded on a ZEISS Ultra Plus FESEM instrument.

UV-vis absorption study

Extinction spectra of the working solution were recorded in SHIMADZU UV-3600 plus UV-VIS-NIR spectrophotometer using an optical quartz cuvette (10 mm path length) over the entire visible range of 200–800 nm. The optical density of the solution was ~0.3 (~6 nM concentration in terms of AuNPs). %T was recorded and then %T was converted to Absorbance as per the equation, Absorbance = 2–log(%T).

Dynamic light scattering (DLS) study

A dynamic light scattering (DLS) study was performed to monitor the dynamic self-assembly process. The change in hydrodynamic diameter of the NPs in each stage was monitored through DLS and measured in Nano ZS90 (Malvern) Zetasizer instrument. The optical density of the NP solution during the self-assembly experiment was kept around ~0.3.

Zeta potential studies

The zeta potential (ζ) of the positively charged AuNPs was measured in milli-Q water (pH~ 7.0) on Nano ZS90 (Malvern) Zetasizer instrument. The optical density of the nanoparticle solution was maintained at ~0.3 during all the measurements. The error was calculated from three different experiments. ζ was determined by measuring the electrophoretic mobility and using Henry's equation.

$$U_E = \frac{2\epsilon\zeta f(K_a)}{3\eta}$$

U_E: Electrophoretic mobility

ζ: Zeta potential

ε: Dielectric constant

η: Viscosity

$f(K_a)$: Henry's Function

Circular Dichroism (CD) study

CD spectra were obtained using a Jasco J815 spectropolarimeter and a cuvette with a 0.1 cm path length. The hexokinase concentration was 4 μM.

High-Performance Liquid Chromatography (HPLC) study

HPLC analysis was carried out using UV-Vis diode array detector equipped Agilent 1260 Infinity-II series high-performance liquid chromatography (HPLC) system. For all reactions, a Phenomenex Kinetex reversed-phase column with dimensions 150×4.6 mm, 2.6 μm EVO C18 was used. The solvents used for the HPLC were 10 mM ammonium acetate buffer pH 6.0 (solvent A) and MeOH (solvent B). A 10 min gradient method with a flow rate of 0.5 mL/min was employed, beginning with 100 % solvent A at 0 min, holding at 100 % solvent A until 2 min, then decreasing to 90 % solvent A from 3 to 8 min, and further increasing to 100 % solvent A until 10 min.

Section 2:

Estimation of the number of TMA ligands

Size of AuNPs used in the study, d = 5.4 nm

Radius of AuNP, r = 2.7 nm

Volume of one AuNP = $\frac{4}{3}\pi r^3$ = 82.4 nm^3

Density of bulk gold = 19.3 g/cm^3

Mass of one AuNP = (82.4 × 10^{-21} × 19.3) g = 1.59 × 10^{-15} mg

Stock: 22.4 mg $HAuCl_4$ is redispersed in 2 mL milli-Q water.

10 µL stock is diluted to 3 mL milli-Q water for the self-assembly study.

Therefore, 3 mL solution contains 0.112 mg $HAuCl_4$ or 0.056 mg Au.

Number of AuNPs in 3 mL = $\frac{0.056\ mg}{1.59 \times 10^{-15} mg}$ = 3.522× 10^{13}

Surface area of one AuNP = 4 $\pi(2.7)^2$ nm^2 = 91.56 nm^2

Thiol footprint = 0.214 nm^2.[4]

Number of TMA ligands on one AuNP = $\frac{91.56\ nm^2}{0.214\ nm^2}$ ~ 428

Therefore, the total number of TMA ligands in 3 mL solution of AuNP = (3.522× 10^{13} × 428)

= 1.5047 × 10^{16}

1 mol TMA = 6.023 × 10^{23} number of TMA ligands

1 nmol TMA = 6.023 × 10^{14} number of TMA ligands

Therefore, total TMA ligands in 3 mL solution = $\frac{1.5047 \times 10^{16}}{6.023 \times 10^{14}}$ = 25.03 nmol = ~ 25 nmol or 8.33 µM

Section 3:

Co-assembly of [+] AuNPs and ATP molecules at different pH conditions

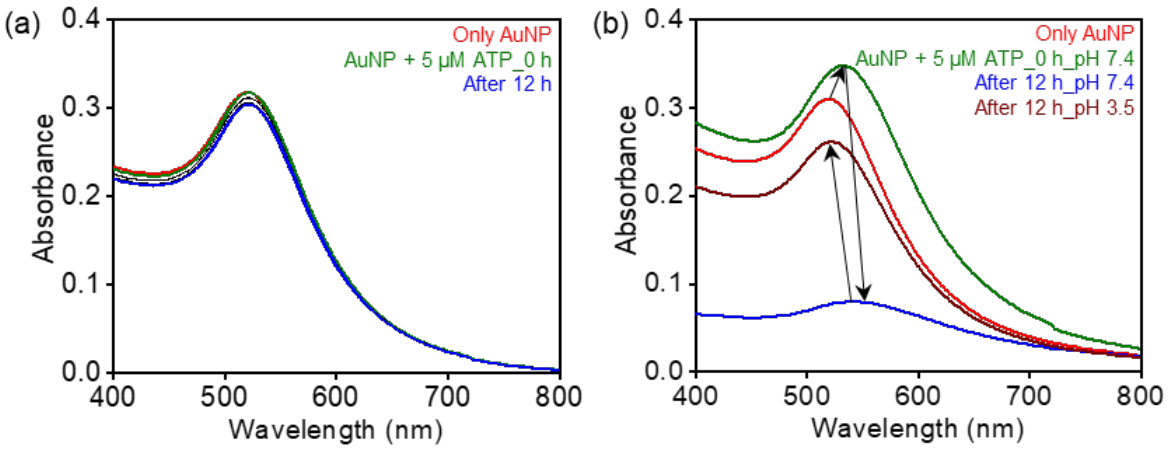

Figure S3. pH tuneable aggregation power of ATP. (a) Absorption data showing negligible aggregation of [+] AuNPs in the presence of ~5 µM ATP at pH ~3.5, even after ~12 h. **(b)** Absorption data showing an instant aggregation of [+] AuNPs in the presence of ~5 µM ATP, when the pH was changed from ~3.5 to ~7.4 (red to green). A complete precipitation was observed within 12 h (green to blue). Further, the reversal of solution pH to ~3.5 results in the complete redispersion of AuNP-ATP precipitates (blue to brown).

Section 4:

Estimation of the threshold concentration of ATP to induce aggregation of ~6 nM AuNPs at pH ~3.5

To determine the minimum concentration of ATP required to induce AuNPs (6 nM) aggregation at pH ~3.5, assembly experiments were conducted using ATP concentrations ranging from 5 to 50 µM. The aggregation process was monitored by tracking changes in λ_{max} over time. At 5 µM ATP, no shift in λ_{max} was observed, indicating the absence of aggregation. Aggregation was first detected at 10 µM ATP, while a pronounced shift in λ_{max} was observed at 50 µM ATP, reflecting significant assembly. These results indicate that the threshold concentration of ATP required to drive AuNPs (6 nM) aggregation at pH 3.5 was 10 µM.

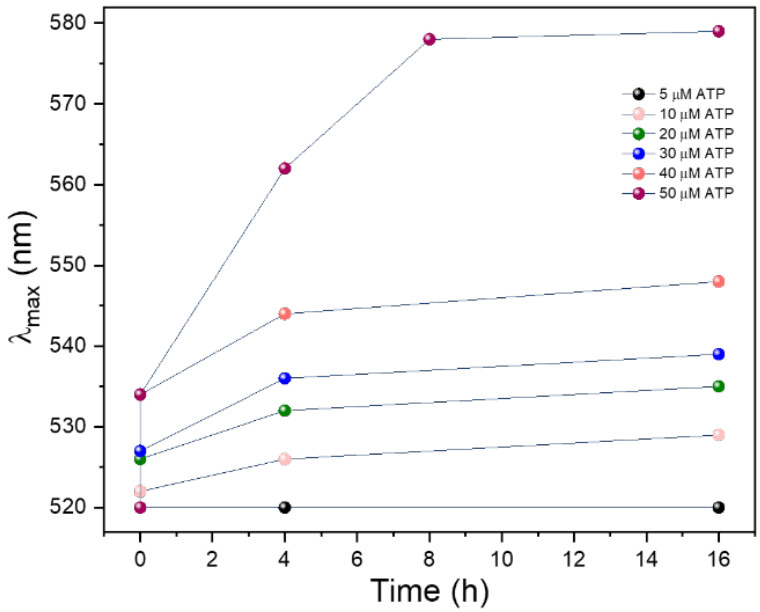

Figure S4. Variation in the λ_{max} of [+] AuNPs (6 nM) in the presence of varying concentrations of ATP at pH 3.5.

Section 5:

Dynamic self-assembly of [+] AuNPs in the presence of 50 µM ATP

Monitoring the self-assembly of [+] AuNP in the presence of 50 µM ATP through UV-vis absorption

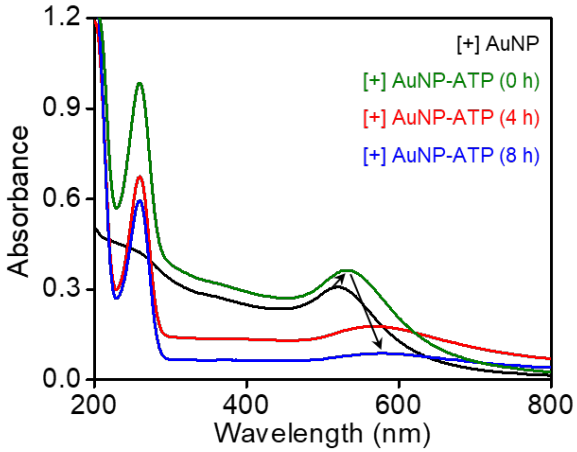

Figure S5. Absorption data depicts an instant aggregation, followed by complete precipitation of [+] AuNPs after adding ~50 µM ATP.

Role of Glucose on the nanoparticle self-assembly

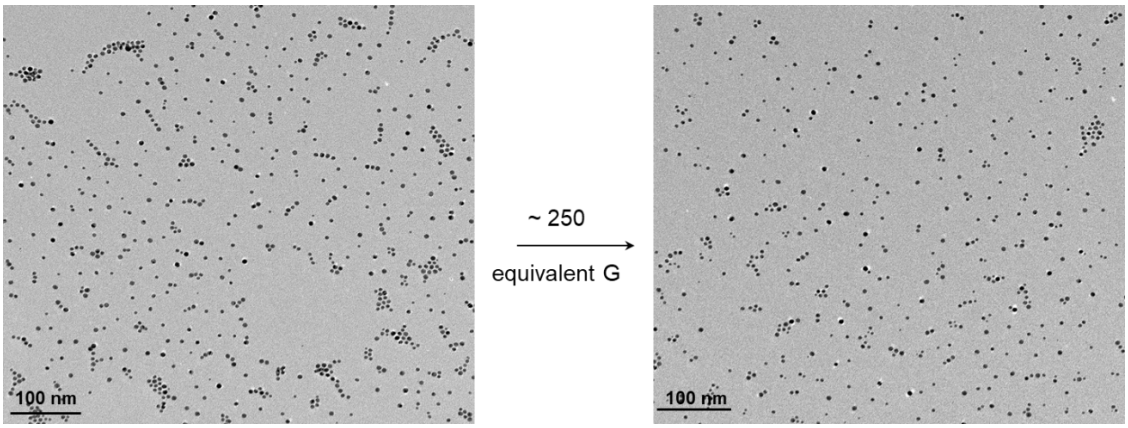

Figure S6. TEM images of AuNPs before and after the addition of ~250 equivalent glucose, confirming the negligible effect of glucose on the nanoparticle self-assembly process.

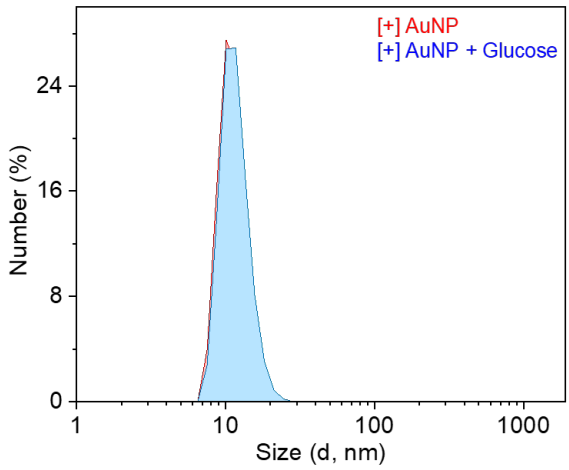

Figure S7. DLS data of AuNPs recorded before and after the addition of ~250 equivalent glucose, confirming the negligible effect of glucose on the nanoparticle self-assembly process.

Monitoring the dynamic self-assembly through DLS

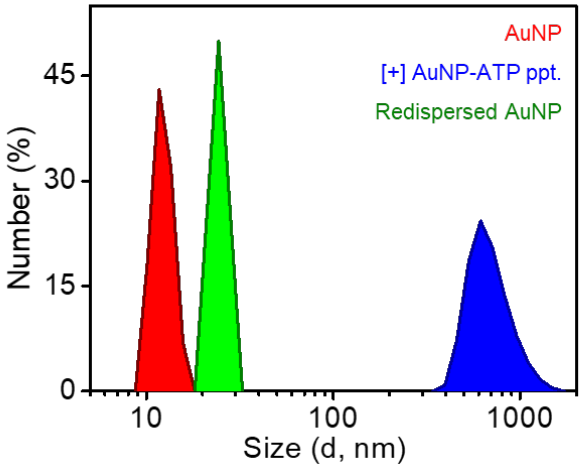

Figure S8. DLS data showing that dispersed AuNPs undergo a self-assembly process upon addition of 50 µM ATP to form the ATP-AuNP precipitate, which eventually redisperses into individual AuNPs in the presence of 5.25 U/3 mL HK enzyme.

It should be noted that the hydrodynamic diameter obtained after redispersion (DLS) is comparable, although not identical, to that measured for AuNPs dispersed in water. This observation does not arise from particle aggregation; rather, it is attributed to the electrostatic association of HK with [+] AuNPs and the accompanied refractive index change.

Monitoring the dynamic self-assembly of AuNPs through SEM

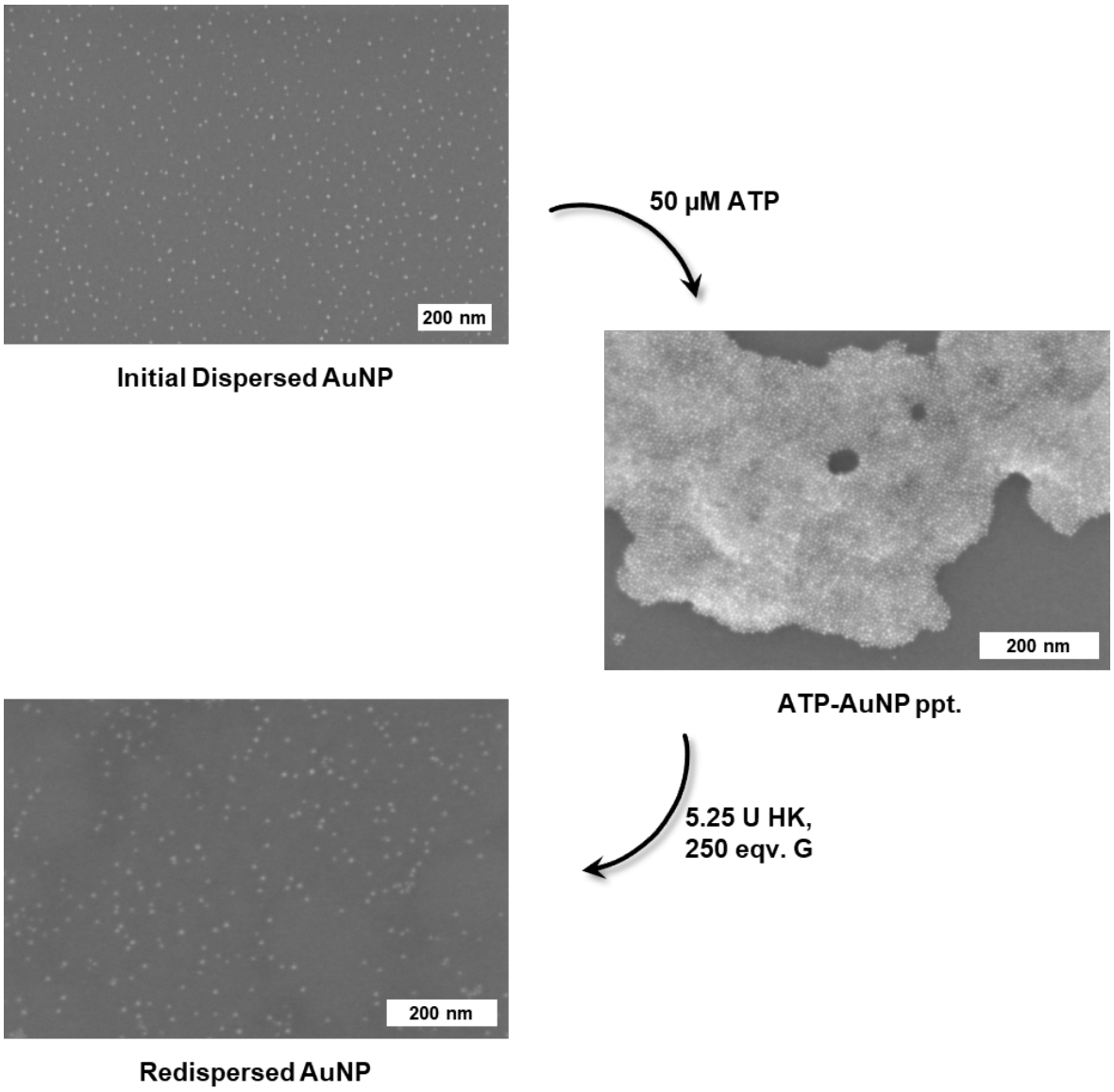

Figure S9. Time-dependent SEM study shows that dispersed AuNPs undergo a self-assembly process to form the ATP-AuNP precipitate, which eventually redisperse in the presence of HK enzyme.

Section 6:

Pathway I: Excess disassembling trigger (HK) driven autonomous reversibility

With 0.36 U HK

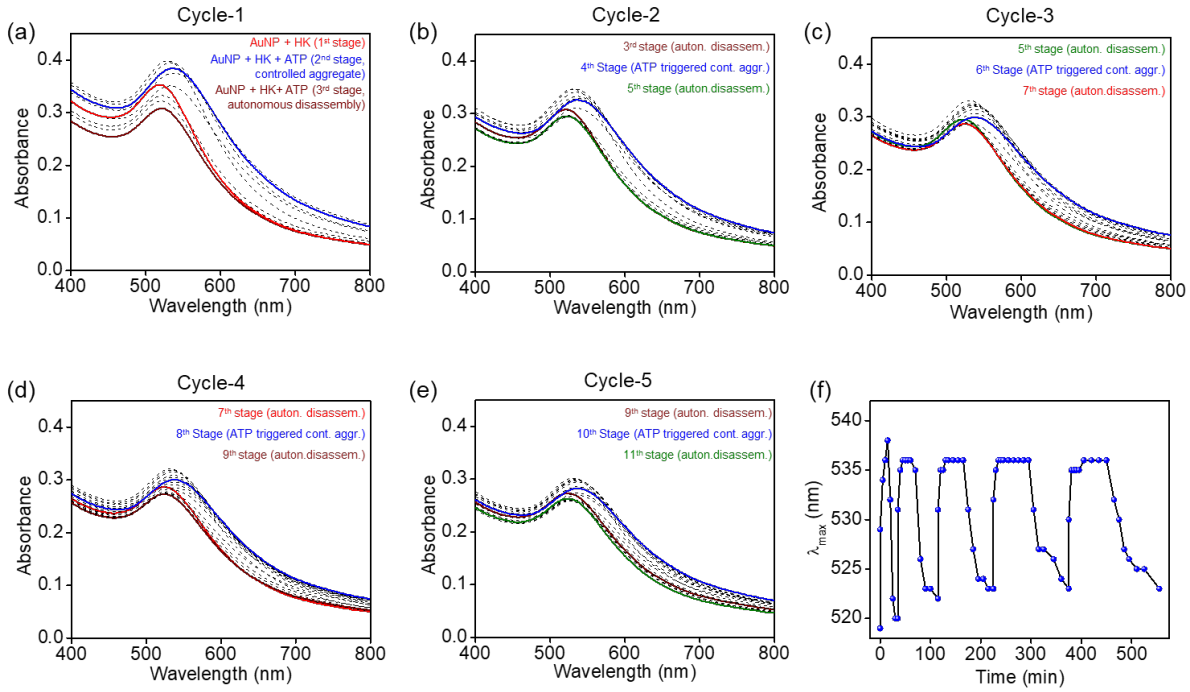

Figure S10. Excess HK-driven autonomous reversibility. The dynamic self-assembled cycles are carried out in 10 mM HEPES buffer (pH ~7.4) with ~6 nM AuNPs, ~0.36 U HK/3 mL, and ~250 equiv. G. 5 µM ATP was added in each cycle to start the self-assembly process. **(a)** Cycle-1 **(b)** Cycle-2 **(c)** Cycle-3 **(d)** Cycle-4 and **(e)** Cycle-5 **(f)** A plot showing the temporal change in the λ_{max} of AuNPs during each cycle of the self-assembly process.

Formation of plasmonically active controlled aggregates in pathway I

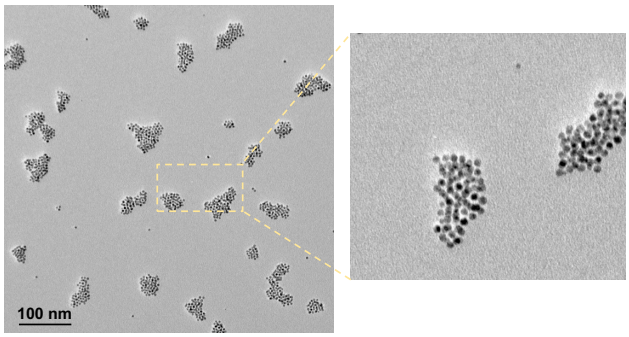

Figure S11. TEM images show that [+] AuNP aggregates formed in pathway I (transiently dispersed) are small-sized and contain a limited number of AuNPs, leading to the formation of plasmonically active controlled aggregates.

with 0.06 U HK

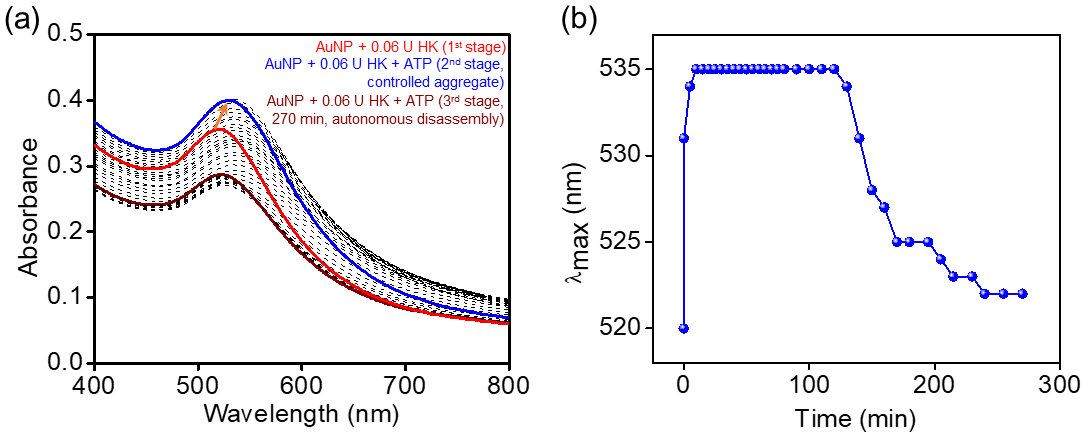

Figure S12. Dynamic self-assembly of [+] AuNPs in the presence of 250 equiv. G. with 0.06 U HK. The kinetics of dynamic self-assembly of [+] AuNPs was carried out using 0.06 U HK amount. **(a)** In a course time of ~270 min, one cycle was observed with 0.06 U HK/3 mL. **(b)** A plot showing the temporal change in the λ_{max} of AuNPs during the self-assembly process.

with 0.18 U HK

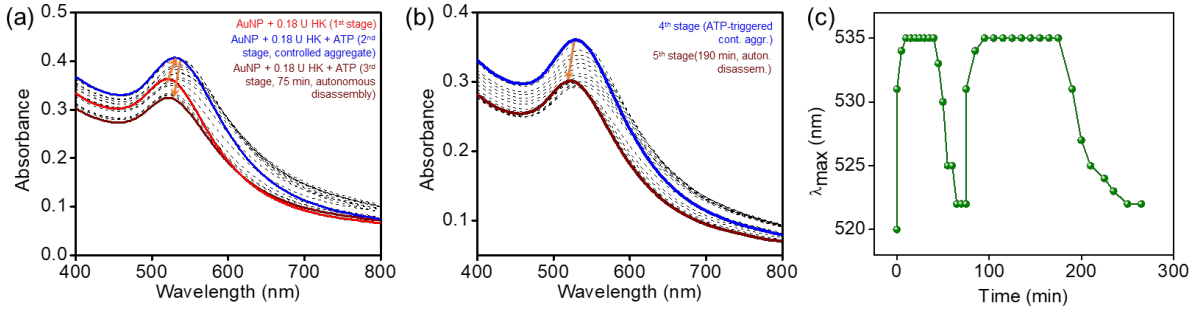

Figure S13. Dynamic self-assembly of [+] AuNPs in the presence of 250 equiv. G. with 0.18 U HK. The kinetics of dynamic self-assembly of [+] AuNPs was carried out using 0.18 U HK amount. **(a, b)** In a course time of ~270 min, two cycles were observed with 0.18 U HK/3 mL **(c)** A plot showing the temporal change in the λ_{max} of AuNPs during each cycle of the self-assembly process.

with 0.36 U HK

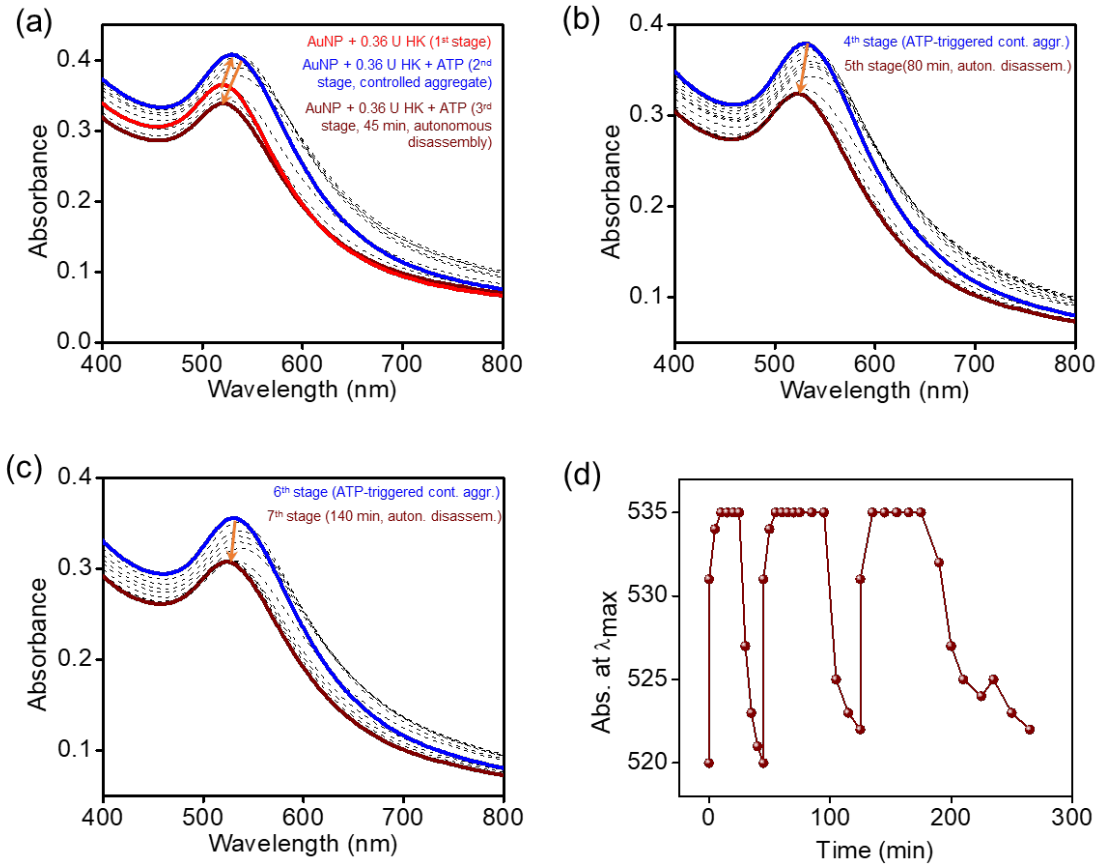

Figure S14. Dynamic self-assembly of [+] AuNPs in the presence of 250 equiv. G. with 0.36 U HK. The kinetics of dynamic self-assembly of [+] AuNPs was carried out using 0.36 U HK amount. **(a-c)** In a course time of ~270 min, three cycles were observed with 0.36 U HK/ 3 mL **(d)** A plot showing the temporal change in the λ_{max} of AuNPs during each cycle of the self-assembly process.

Section 7:

Dynamic self-assembly of [+] AuNPs in the presence of 250 µM ATP

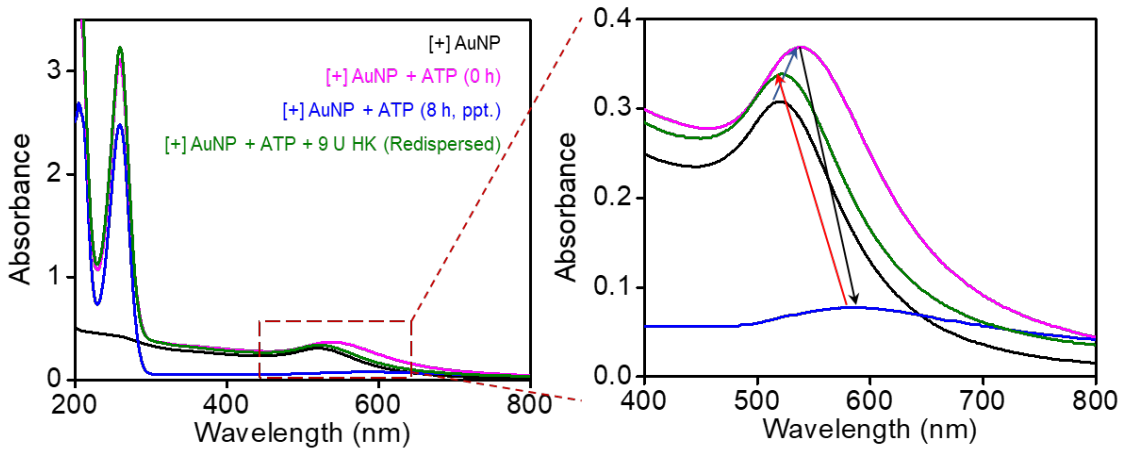

Figure S15. Absorption data depict an instant aggregation, followed by complete precipitation of [+] AuNPs after adding ~250 µM ATP. Addition of 9U HK/3 mL led to complete redispersion of AuNPs.

Electrostatic proximity of HK on the surface of AuNPs

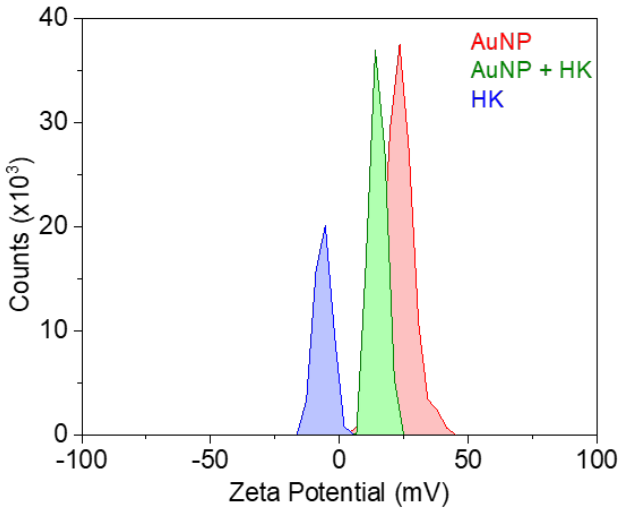

Figure S16. Zeta potential of [+] AuNPs decreased from 25.5 ± 2.1 mV to 14.2 ± 1.7 mV upon addition of 3 units of HK, proving the electrostatic proximity of HK on the surface of AuNPs.

Mechanistic details in pathway II:

Activity of HK at pH 3.5: The HK is known to show pH-dependent activity, with maximum activity at physiological pH ~7.4. Bhat and co-workers have reported that at pH 3.5, HK largely preserves its native secondary structure but undergoes partial disruption of tertiary interactions,

leading to a compact molten globule–like state.[5] In this conformation, the enzyme retains limited catalytic activity, while full denaturation and loss of function occur only at pH values below 2.5.

To assess the pH-dependent activity of the HK enzyme, we also carried out a stability study as a function of pH and time. The circular dichroism (CD) spectra were recorded in the range of 200-250 nm, which indicates changes in the enzyme's folding (typically the α-helix signal at 222 nm) as pH and time varied. As reported by Bhat and co-workers, we also did not observe any significant change in the CD spectra of HK at pH 3.5 and 7.4. Further, the enzyme stability was monitored over time at the working pH of 3.5. Initially, no significant change in the CD signal was observed up to 30 min. Afterwards, a gradual decrease in the CD (mdeg) value at 222 nm (from 60 to 240 min) was observed, followed by a larger change at 360 min (although the feature of minima at 222 nm is still maintained). Thus, HK largely preserves its native secondary structure at pH 3.5 initially; however, over time, it gradually loses stability and enzymatic activity.

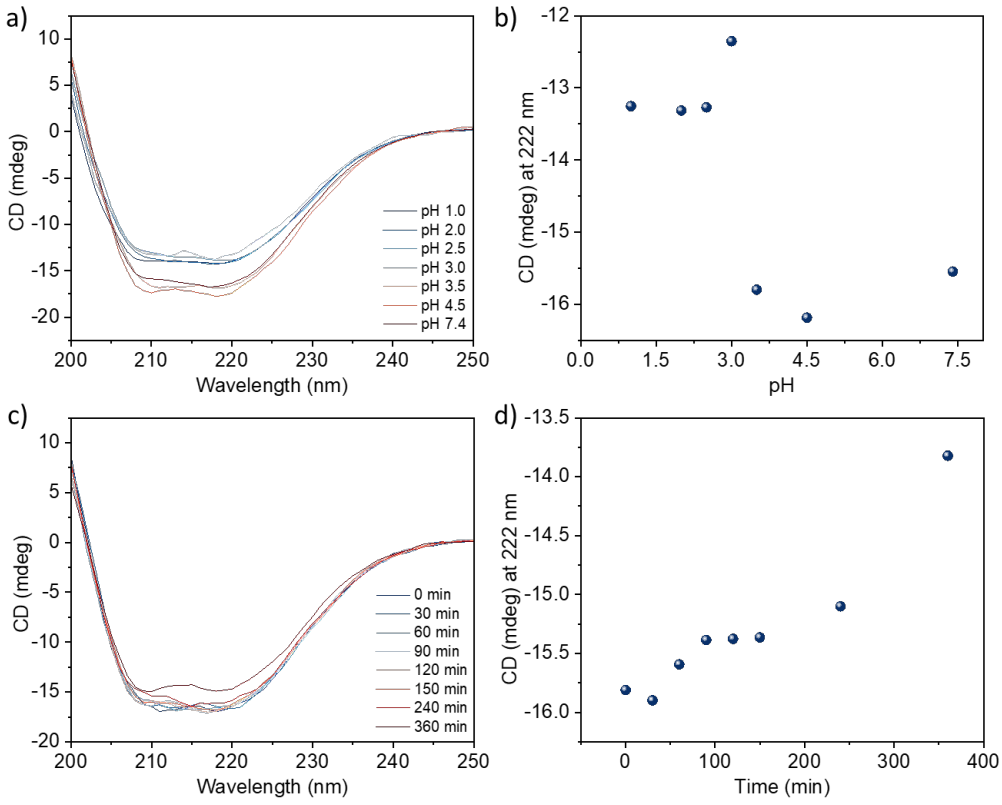

Figure S17. Stability of HK enzyme as a function of pH and time. **(a)** Circular dichroism, CD (mdeg), spectra at varying pH. **(b)** CD signal at 222 nm as a function of pH, showing no significant change at pH 3.5 relative to pH 7.4. **(c)** Time-dependent CD (mdeg) spectra at pH 3.5. **(d)** CD signal at 222 nm at pH 3.5 as a function of time, showing a gradual decrease in the CD (mdeg) value at 222 nm (from 60

to 240 min) was observed, followed by a larger change at 360 min (although the feature of minima at 222 nm is still maintained).

As reported by Bhat and co-workers, HK adopts a molten globule state at pH 3.5, where the active site cleft partially collapses, making it difficult but not impossible for glucose to enter and bind.[5] Additionally, the protonation of key acidic residues further weakens the enzyme's grip on the substrate. Having said that, sufficient structural integrity is retained at pH 3.5, allowing for occasional, low-affinity binding events. This enables the enzyme to maintain its ATP to ADP conversion ability, even though the catalytic conversion is significantly less efficient than at physiological pH ~7.4. This is also evident from the current study, where a complete redispersion of precipitated AuNPs (**Fig. 1a-c**) was observed after the addition of a threshold amount of HK (5.25 units for 50 μM ATP). Time-resolved ^{31}P NMR spectroscopy (**Fig. 1d**) confirms that HK retains partial catalytic activity at pH 3.5. A progressive decrease in the β-phosphate resonance of ATP (~23 ppm) was observed, along with the appearance of signals corresponding to glucose-6-phosphate (~1 ppm) and inorganic phosphate (~0.05 ppm). These spectral changes clearly demonstrate the coupled dephosphorylation of ATP to ADP and the phosphorylation of glucose to glucose-6-phosphate. Therefore, under our experimental conditions, the HK enzyme may be partially denatured at pH 3.5, but it still maintains limited catalytic activity. However, due to significant loss of activity over time under the working conditions of pathway II (pH 3.5), HK behaves less as an efficient catalyst and more as a stoichiometric reagent. This explains why the addition of HK does not monotonically lead to the thermodynamic endpoint of a dispersed state, and a complete redispersion of AuNPs was observed only after the addition of a threshold amount of HK in the system.

In Pathway II, the addition of a larger quantity of enzyme (9 units of HK) leads directly to the complete redispersion of AuNPs (**Fig. S18**).

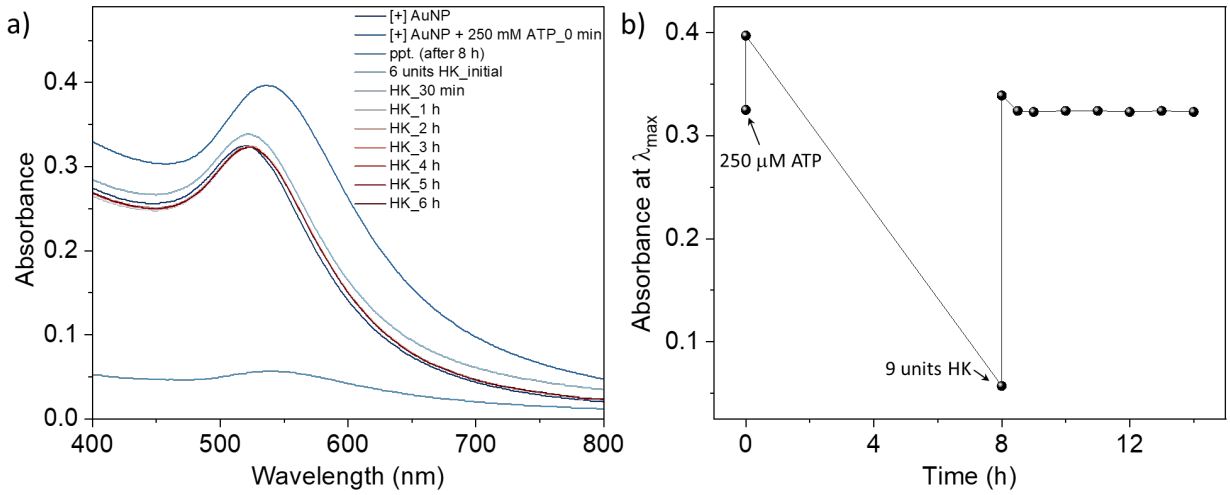

Figure S18. Spectra changes in the **(a)** UV-vis absorption and **(b)** absorbance at λ_{max} of [+] AuNPs with time in the presence of 9 units of HK.

Role of glucose concentration on the disassembly step in pathway II

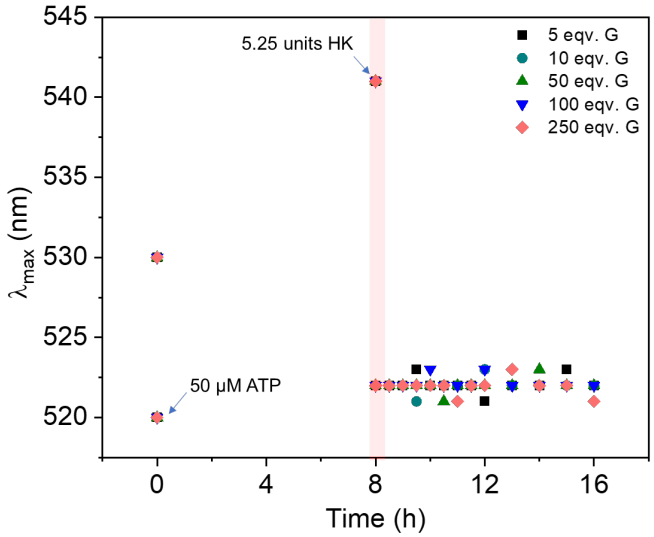

Figure S19. Effect of glucose concentration on the disassembly step in pathway II. Variation in the λ_{max} of [+] AuNPs with time in presence of varying concentration of glucose. Addition of 250 µM ATP resulted in the complete precipitation of [+] AuNP within ~8h. Afterwards, 3 units of HK and varying concentrations of glucose was added to disassemble the precipitated AuNPs. No significant change in the time of disassembly was observed as a function of glucose concentration (region after 8 h).

Section 8:

Pathway II: Excess aggregating trigger (ATP) driven autonomous reversibility

with 250 µM ATP

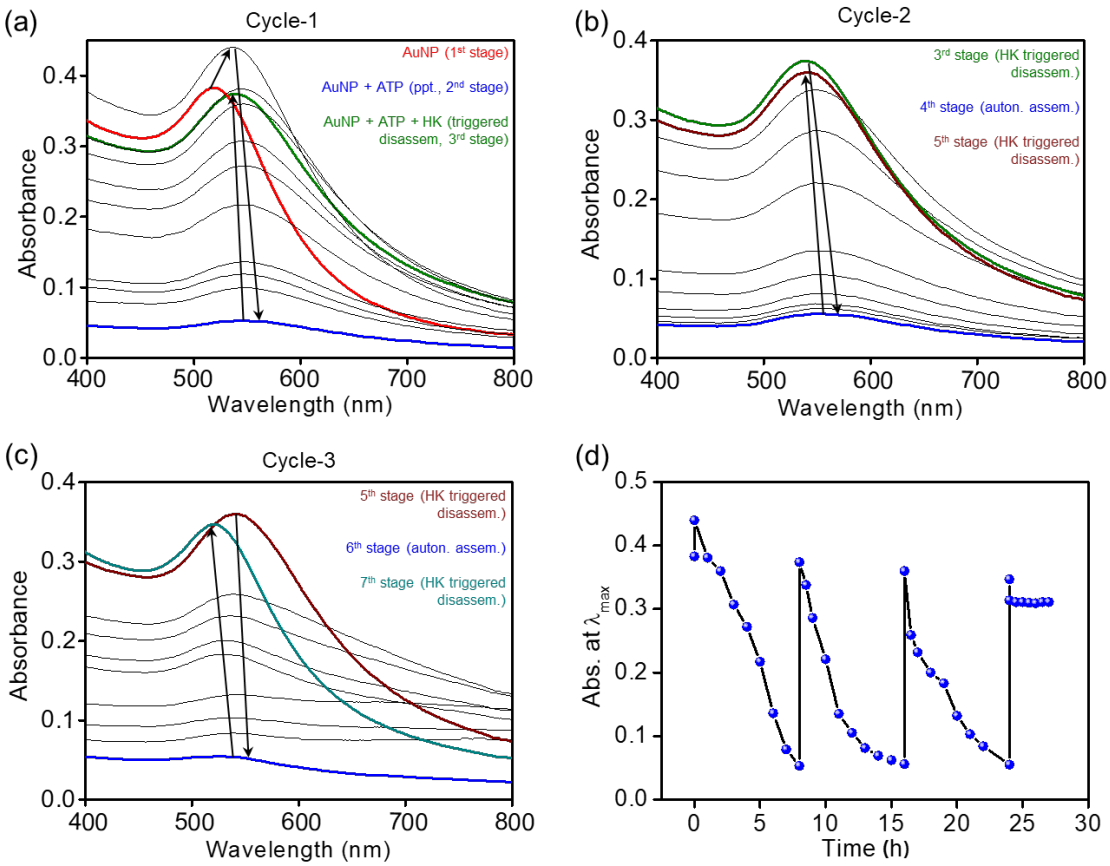

Figure S20. (a-c) 250 µM ATP-triggered dynamic self-assembly of AuNPs yielded 3 cycles of autonomous-assembly — triggered-disassembly. **(d)** A plot showing the temporal change in the λ_{max} of AuNPs during each cycle of the self-assembly process.

with 350 µM ATP

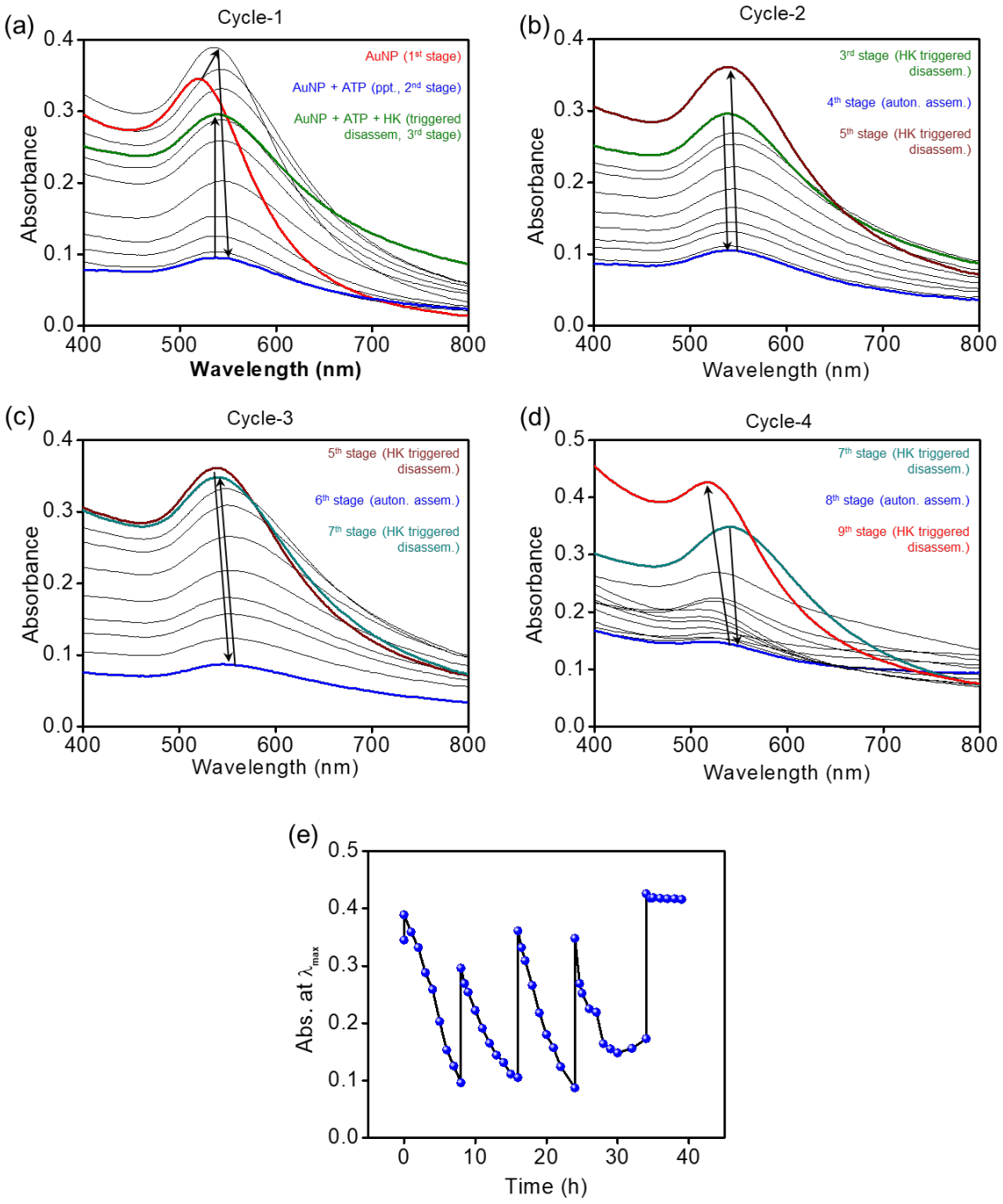

Figure S21. (a-d) 350 µM ATP-triggered dynamic self-assembly of AuNPs yielded 4 cycles of autonomous-assembly — triggered-disassembly. **(e)** A plot showing the temporal change in the λ_{max} of AuNPs during each cycle of the self-assembly process.

with 500 µM ATP

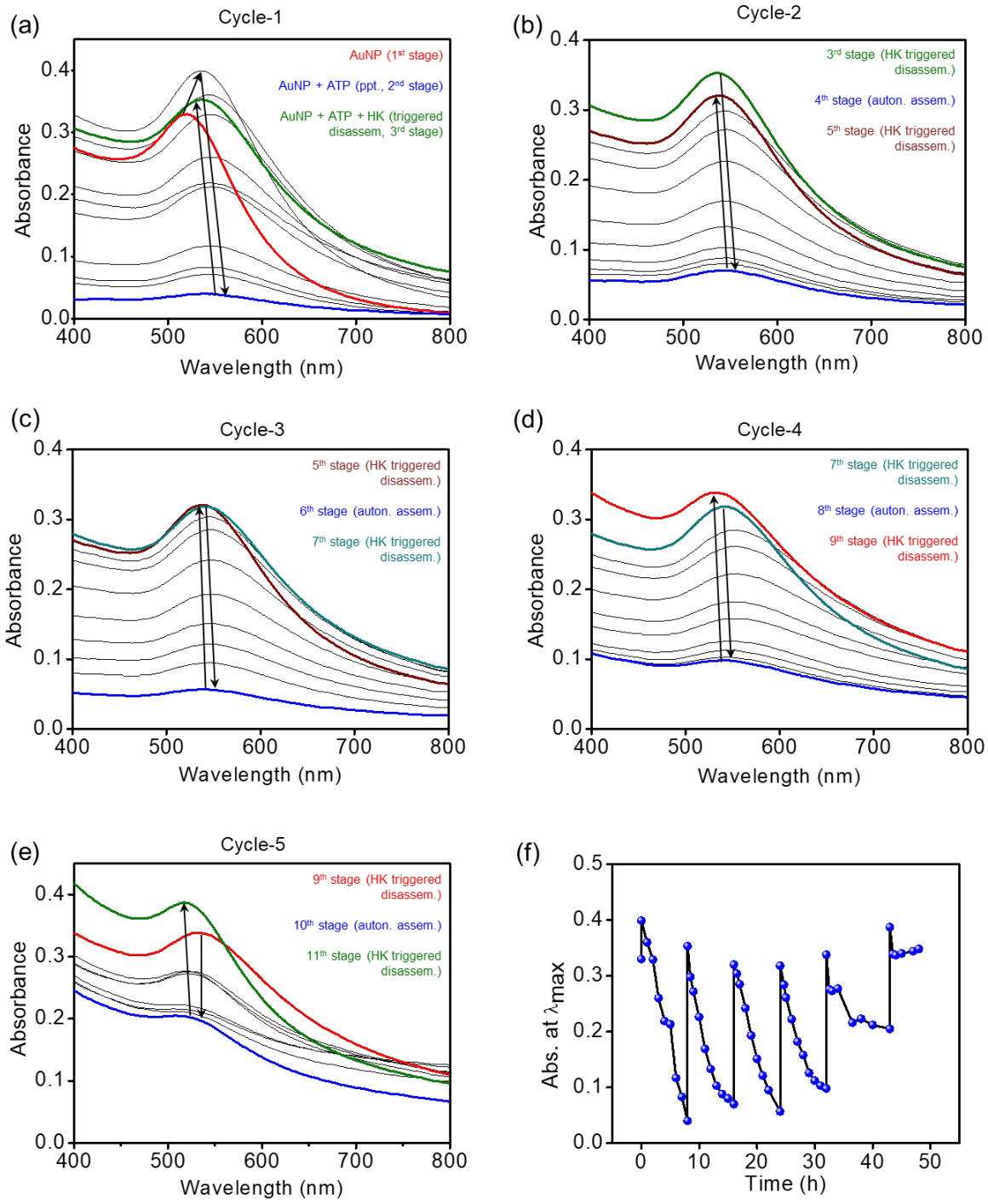

Figure S22. (a-e) 500 µM ATP-triggered dynamic self-assembly of AuNPs yielded 5 cycles of autonomous-assembly — triggered-disassembly. **(f)** A plot showing the temporal change in the λ_{max} of AuNPs during each cycle of the self-assembly process.

with 750 µM ATP

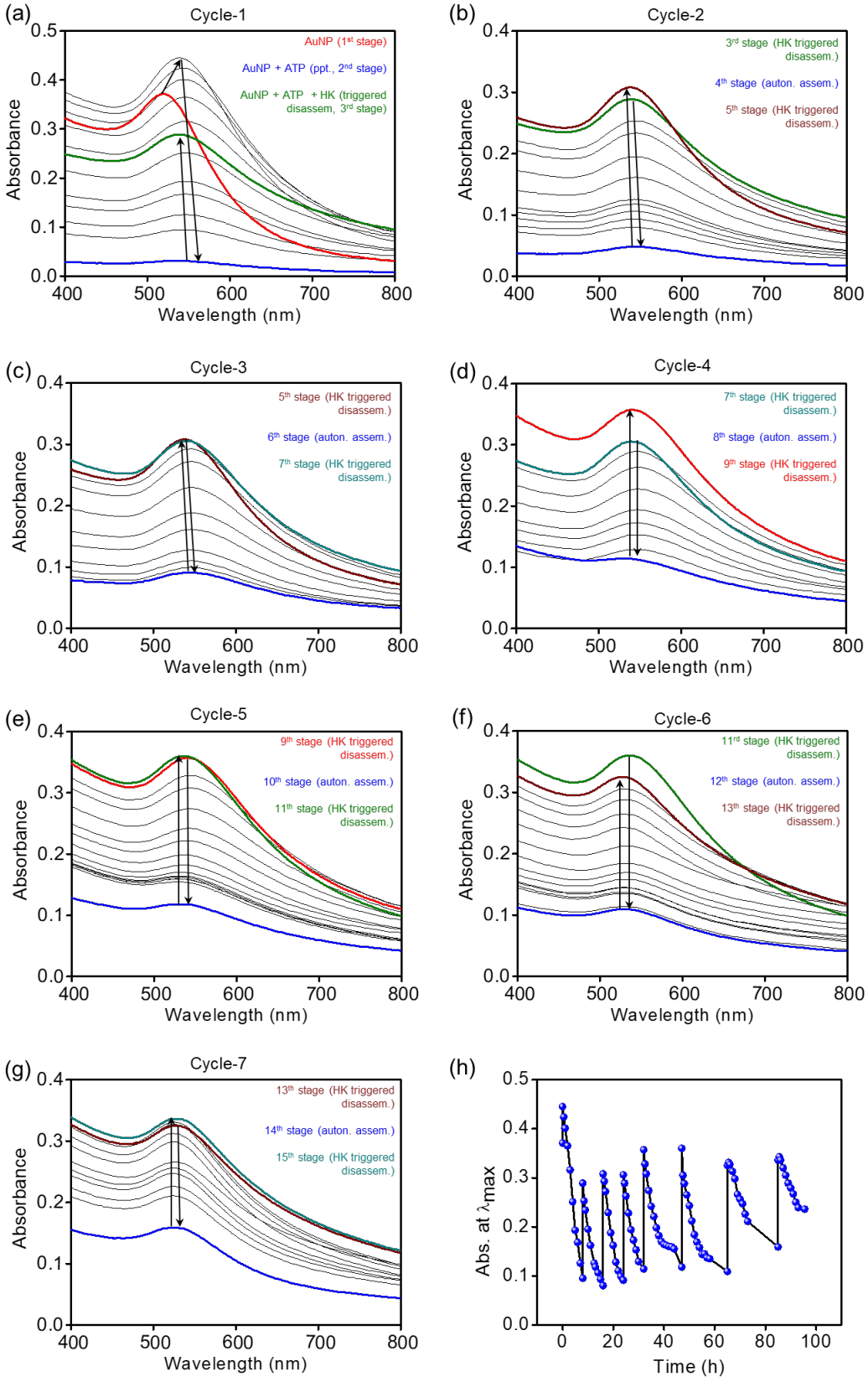

Figure S23. (a-g) 750 µM ATP-triggered dynamic self-assembly of AuNPs yielded 7 cycles of autonomous-assembly — triggered-disassembly. **(h)** A plot showing the temporal change in the λ_{max} of AuNPs during each cycle of the self-assembly process.

with 1 mM ATP

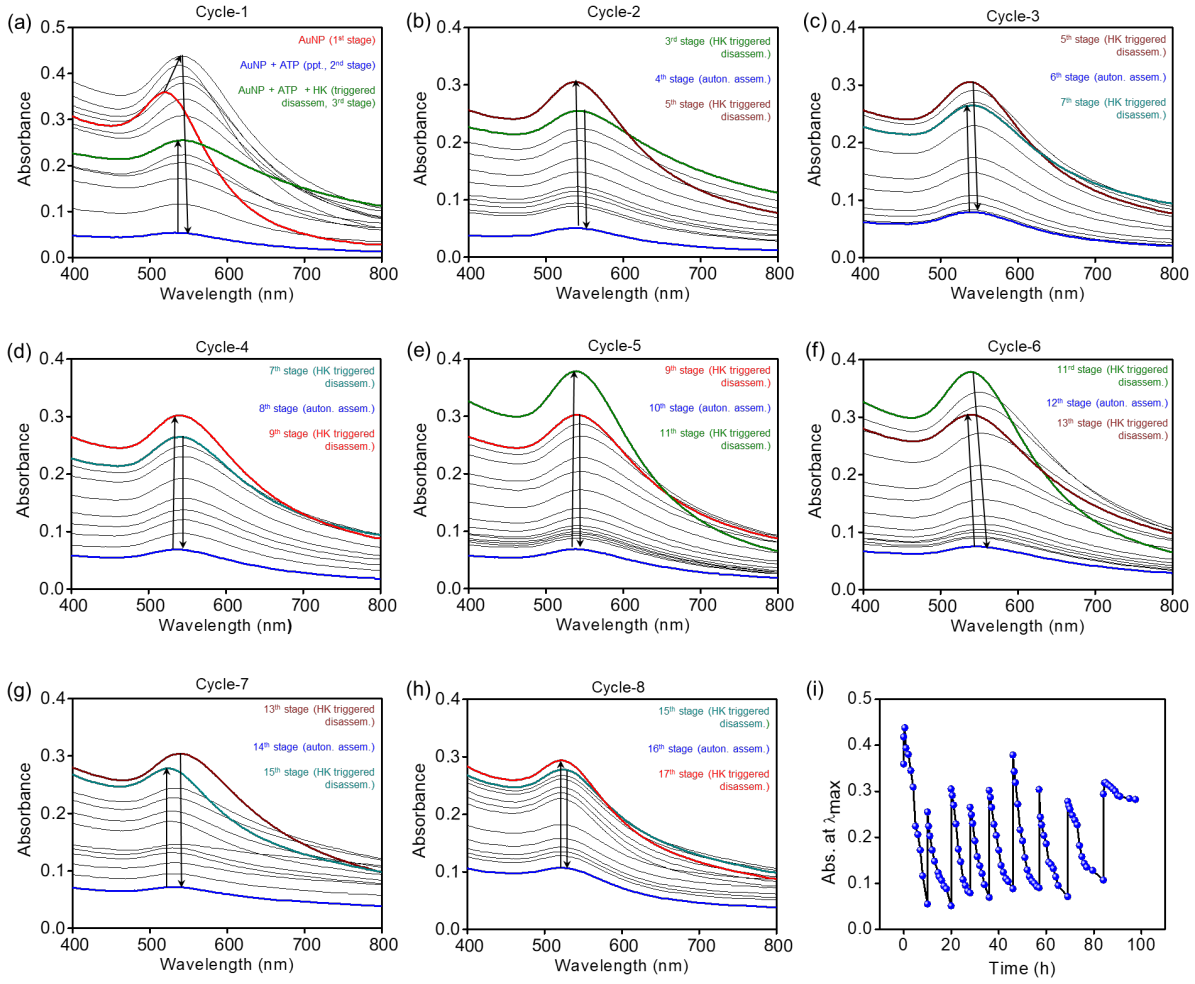

Figure S24. (a-h) 1 mM ATP-triggered dynamic self-assembly of AuNPs yielded 8 cycles of autonomous-assembly — triggered-disassembly. **(i)** A plot showing the temporal change in the λ_{max} of AuNPs during each cycle of the self-assembly process.

Conversion percentage of ATP to ADP:

HPLC studies were performed to estimate the conversion percentage of ATP to ADP after each cycle. It is to be noted that the separation of ATP and ADP is challenging and often results in coelution in HPLC, due to the minimal polarity difference between the two nucleotides. Despite our extensive efforts, a partial overlap between the chromatograms of ATP and ADP peaks persists, influencing the exact quantification (**Fig. S25**). Hydrolysis of 250 µM ATP solution was performed by adding 3 units of HK in each cycle, and the corresponding chromatograms were collected. HPLC chromatograms clearly show the progressive conversion of ATP to ADP

upon batchwise addition of 3 units of HK enzyme, with a complete conversion after the third cycle.

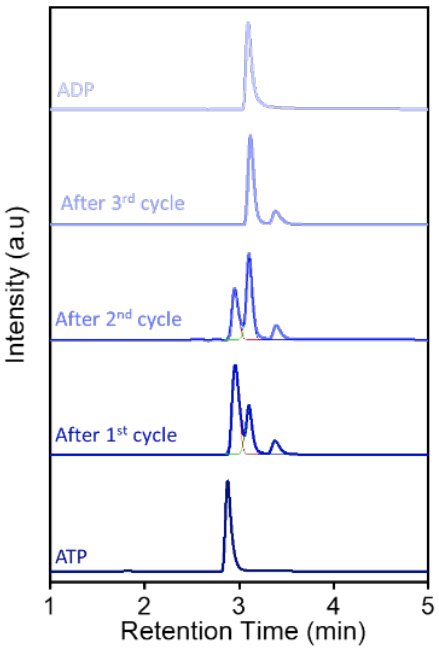

Figure S25. HPLC study showing the progressive conversion of ATP to ADP upon batchwise addition of 3 units of HK enzyme in each cycle at pH 3.5. The initial concentration of ATP was 250 µM.

References

1. J. Tien, A. Terfort and G. M. Whitesides, *Langmuir* 1997, **13**, 5349-5355.

2. N. R. Jana and X. Peng, *J. Am. Chem. Soc.* 2003, **125**, 14280-14281.

3. A. Rao, S. Roy, M. Unnikrishnan, S. S. Bhosale, G. Devatha and P. P. Pillai, *Chem. Mater.* 2016, **28**, 2348-2355.

4. J. Green, J. J. Stokes, G. D. Wignall, G. L. Glish, M. D. Porter, N. D. Evans and R. W. Murray, *Langmuir* 1998*, **14**, 17-30*)

5. P. Kumar, A. Tiwari and R. Bhat, *J Biol Chem*. 2004, **279**, 32093–32099.